Springer

Journal of
Mechanical
Science and
Technology

Journal of Mechanical Science and Technology 22 (2008) 320~329

www.springerlink.com/content/1738-494x

Numerical and experimental study on hollow-cone fuel spray of high-pressure swirl injector under high ambient pressure condition

Young-Sam Shim[1], Gyung-Min Choi[2,*] and Duck-Jool Kim[2]

[1]*Research Institute of Mechanical Technology, Pusan National University, Busan 609-735, Korea*
[2]*Pusan Clean Coal Center, Pusan National University, Busan 609-735, Korea*

(Manuscript Received February 20, 2007; Revised October 24, 2007; Accepted October 25, 2007)

Abstract

A hybrid breakup model was proposed as a trustworthy prediction of hollow-cone fuel spray in the present study and the atomization process of the hollow-cone fuel spray of a high-pressure swirl injector in a Gasoline Direct Injection (GDI) engine under high ambient pressure conditions was studied by a new hybrid breakup model. The proposed hybrid breakup model is composed of the Linearized Instability Sheet Atomization (LISA) model as a primary breakup process. The Aerodynamically Progressed Taylor Analogy Breakup (APTAB) model, instead of the Taylor Analogy Breakup (TAB) model, was used as a secondary breakup process. The effects of the droplet deformation on a droplet aerodynamic external force are considered in the APTAB model. In addition, we replaced the x^2 distribution function used in previous the APTAB model by the Rosin-Rammler distribution function to improve the prediction precision. The Laser Induced Exciplex Fluorescence (LIEF) technique and the Phase Doppler Anemometry (PDA) system were used to produce a set of experimental data for the model validation. The estimation of the prediction ability of the LISA+APTAB model was carried out, and spray characteristics, which are difficult to obtain by experimental method, were calculated and discussed. The suggested hybrid breakup model showed better prediction capability compared with the previous model (LISA+TAB model). From the calculated results, the effect of the ambient pressure on the SMD (Sauter Mean Diameter) and droplet velocity could be discussed quantitatively.

Keywords: GDI (Gasoline Direct Injection); Hybrid breakup model; Atomization; LISA (Linearized Instability Sheet Atomization) model; APTAB (Aerodynamically Progressed Taylor Analogy Breakup) model; SMD (Sauter Mean Diameter)

1. Introduction

Gasoline Direct Injection (GDI) engines offer great potential for improvements in fuel economy, transient control, performance, and emissions over Port Fuel Injection (PFI) engines. These advantages are dependent on adequate spray atomization, mixture formation and concentration inside the cylinder. Therefore, a suitable fuel injector is needed to provide effective control of the spray motion and to satisfy the basic requirements for atomization and mixing. Among various injectors, high-pressure swirl injectors have been most commonly used in GDI engines. This high-pressure swirl injector produces a hollow-cone fuel spray by providing a swirl rotational motion to the fuel inside the injector, and generates a widely dispersed and well-atomized spray even for lower injection pressure. To apply this high-pressure swirl injector to various GDI engines effectively, a detailed understanding of spray characteristics of the high-pressure swirl injector is essential.

Many researchers have tried to understand the spray characteristics, such as the spray structure, SMD, droplet velocity and spray tip penetration, experimentally. Evers [1] reported that a transient swirl spray could be divided into four regions: the leading edge, the cone, the trailing edge and the vortex cloud. Zhao et al. [2] visualized a spray development proc-

*Corresponding author. Tel.: +82 51 510 2476, Fax.: +82 51 512 5236
E-mail address: choigm@pusan.ac.kr
DOI 10.1007/s12206-007-1044-3

ess of GDI injector by the Mie-Scattering method and measured the Sauter Mean Diameter (SMD) by the Phase Doppler Particle Analyzer (PDPA) system. They also observed that the spray tip penetration and the spray width decreased under high ambient pressure conditions. Preussner et al. [3] investigated the basic mechanisms of interaction between droplets and air over a hollow-cone fuel spray. In their study, after the primary breakup, momentum exchange between the droplets and air leads to a dynamic vacuum in the inner part of the cone. This effect generates a secondary air flow into the spray cone, which supports the stratified charge. Wicker et al. [4] found that the higher injection pressure caused a longer spray tip penetration and wider spray angle from the understanding of the instantaneous and transient GDI spray structure and evolution by the digital particle image velocimetry. Choi et al. [5] studied the spray structure of a vaporizing GDI spray using the Exciplex Fluorescence method. They found that the ambient pressure had a significant effect on the axial growth of the spray, while the ambient temperature had a great influence on the radial growth. Although many experimental studies have been performed, numerical studies are also needed to predict the spray characteristics in the development of new conceptual GDI engines, and to obtain a more detailed understanding of hollow-cone fuel spray under various ambient pressure conditions.

Numerical studies of the spray breakup process have been carried out mainly by using the analytical model. O'Rourke et al. [6] suggested the Taylor analogy breakup (TAB) model, which is based on the analogy between an oscillating and distorting droplet and a spring mass system. Ibrahim et al. [7] suggested the Droplets Deformation and Breakup (DDB) model. In this model, the liquid drop is deformed due to a pure extensional flow from an initial spherical shape into an oblate spheroid of an ellipsoidal cross section. Non-linear effects, which are omitted in the TAB model, are also considered. Park [8] proposed the Aerodynamically Progressed Taylor Analogy Breakup (APTAB) model by considering the effects of droplet deformation on the aerodynamic external force of the droplet. However, these breakup models, which consider only one single breakup model, are insufficient to accurately predict the atomization process of a hollow-cone fuel spray. Hence, to improve the calculation precision, various hybrid breakup models have been developed by combining two different models, such as the WB+TAB model [9], LISA+TAB model [10] and LISA+DDB model [11]. However, these hybrid breakup models still have discrepancies between the calculated and experimental results under high ambient pressure conditions [12]. Therefore, it is necessary to develop a new hybrid breakup model that can predict the spray characteristics of hollow-cone fuel spray under high ambient pressure conditions.

In the present study, a hybrid breakup model for the modeling of hollow-cone fuel spray is suggested. The atomization process of the high-pressure swirl injector in the GDI engine under high ambient pressure conditions was studied by this hybrid breakup model. The hybrid breakup model consists of the LISA model for the primary breakup process and the APTAB model for the secondary breakup process. In addition, we replaced the χ^2 distribution function in the APTAB model with the Rosin-Rammler distribution function. The calculation of the GDI spray characteristics, such as the spray development process, spray tip penetration, droplet axial velocity, ambient gas velocity and SMD, was performed at the ambient pressures of 0.1 MPa, 0.5 MPa and 1.0 MPa for the ambient temperature of 293 K. The estimation of the application possibility of the LISA+APTAB model was performed by comparing it with the experimental data. The LIEF technique and the PDA system were used to produce a set of experimental results for model validation.

2. Experimental setup and method

2.1 Experimental setup

Fig. 1 shows a schematic diagram of the experimental setup of the LIEF technique used for investigating the spray characteristics of the GDI injector. The spray chamber was designed to measure the behavior and structure of the hollow-cone fuel spray under various ambient conditions. The possible maximum ambient temperature and pressure are 600 K and 3 MPa, respectively. Nitrogen was purged as the ambient gas to prevent the quenching of liquid fluorescence by oxygen. The fourth harmonic of the Nd:YAG at 266 nm with duration of 7 ns and a laser energy of 50 mJ/pulse was used to excite dopants from the fuel sprays. The laser beam formed a thin light sheet of 60 mm high and less than 400 ㎛ thick. The filters was 400±25 nm for liquid phase. An additional WG280 sharp cut filter was used to eliminate

the light at 266 nm. The spray images were digitally recorded with an intensified CCD camera that provided 640 by 480 pixel images at a resolution of 8 bits and was mounted perpendicular to the laser sheet. The camera system consisted of a personal computer with an image grabber, a shutter controller, and a pulse generator. In order to inject the fuel with high pressure and to avoid pressure fluctuations in the fuel rail, a compressed nitrogen cylinder and hydraulic accumulator were used. A high pressure swirl injector with 70° was used.

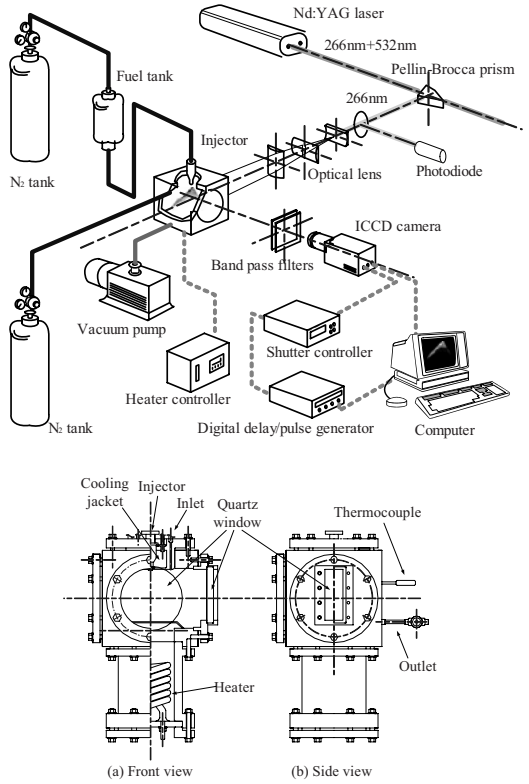

Fig. 1. Experimental setup for the LIEF technique and constant volume chamber.

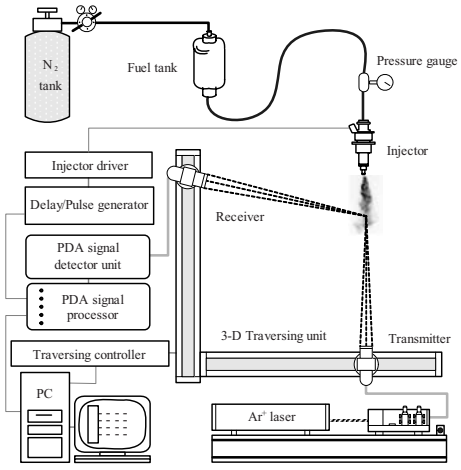

Fig. 2. The PDA system.

Fig. 2 shows the PDA system for measurement of the droplet velocity and SMD. The PDA system consisted of a conventional Dantec fiber optic transmission unit coupled with a standard receiving unit. A 4W Argon-ion laser was used.

2.2 Experimental method

In the LIEF technique, the exciplex system of fluorobenzen and DEMA in a non-fluorescing base fuel of hexane was employed. The boiling points for hexane, fluorobenzene, and DEMA are 338 K, 342 K and 358 K, respectively, and the solution was composed of 89% hexane, 2% fluorobenzene and 9% DEMA by volume.

The green (514.5 nm) laser line was used to provide the vertical droplet velocity and the phase difference for particle sizing in the PDA system. The focal lengths of transmitter and receiver were 400 mm. A scattering angle of 30° was used. The transmission and receiving optical units were mounted on a heavy-duty three-dimensional traverse.

The experimental conditions are shown in Table 1. The injection pressure was kept at 5.1 MPa for all experimental conditions. The injection duration and quantity were 2 ms and 15 mg, respectively, which corresponds to a medium speed and load in GDI engines. Three different ambient pressures of 0.1 MPa, 0.5 MPa and 1.0 MPa under an ambient temperature of 293 K were set.

Table 1. Experimental and calculating conditions.

Fuel	Hexane
Injection pressure (MPa)	5.1
Injection duration (ms)	2.0
Injection quantity (mg)	15
Ambient gas	N_2
Ambient temperature (K)	293
Ambient pressure (MPa)	0.1, 0.5, 1.0

3. Numerical method

3.1 Hybrid breakup model

3.1.1 LISA model (primary breakup model)

The LISA model [10] proposed was used for the primary breakup process. This model is divided into three stages: film formation, sheet breakup, and atomization.

The liquid centrifugal motion inside the injector generates an air core surrounded by liquid film. The thickness of this film is related to the mass flow rate measured experimentally.

$$\dot{m} = \pi\rho u t\left(d_0 - t\right) \tag{1}$$

In equation (1), u is the axial component of velocity at the injector exit. The total velocity is assumed to be related to the injector pressure.

$$U = k_v\sqrt{\frac{2\Delta p}{\rho_l}} \tag{2}$$

where k_v is expressed by Eqn. (3).

$$k_v = \left[0.7,\ \frac{4\dot{m}}{\pi d_0^2\rho_l\cos(\theta)}\sqrt{\frac{\rho_l}{2\Delta p}}\right] \tag{3}$$

In sheet breakup, the sheet will break up and ligaments will be formed at a length given by

$$L = U\tau = \frac{U}{\Omega}\ln\left(\frac{\eta_b}{\eta_0}\right)\frac{-b\pm\sqrt{b^2-4ac}}{2a} \tag{4}$$

where the quantity $\ln\left(\eta_b/\eta_0\right)$ is 12, is based on the work of Dombrowski and Hooper [13].

The diameter of the ligaments formed at the point of breakup can be obtained from a mass balance. If it is assumed that the ligaments are formed from tears in the sheet, once per wavelength, the resulting diameter is given by

$$d_L = \sqrt{\frac{16h}{K_s}} \tag{5}$$

where K_s is the wave number corresponding to the maximum growth rate Ω.

If breakup occurs when the amplitude of the unstable waves is equal to the radius of the ligament, one droplet will be formed per wavelength. A mass balance then gives

$$d_D^3 = \frac{3\pi d_L^2}{K_L} \tag{6}$$

where K_L is now determined from

$$K_L d_L = \left[\frac{1}{2} + \frac{3\mu_l}{2\left(\rho_l\sigma d_L\right)^{1/2}}\right]^{\frac{1}{2}} \tag{7}$$

This is Weber's result for the wave number corresponding to the maximum growth rate for the breakup of a cylindrical, viscous liquid column.

3.1.2 APTAB model (secondary breakup model)

The APTAB model [8] proposed was used for the secondary breakup process. In this model, it is discovered that the deformed droplet shape is an oblate spheroid having an ellipsoidal cross section with a major semi-axis, a, minor semi-axis, b in Fig. 3. Hence, the aerodynamic drag force of the droplet is proportional to the droplet normal cross section area, πa^2. It is also assumed that the aerodynamic external force is proportional to $\rho_g u^2 a^2$ in the APTAB model, while the aerodynamic external force is proportional to ${\rho_g}^2 u^2 r^2$ in the TAB model. The model equation is given by

$$\ddot{y} + \frac{5N}{\mathrm{Re}K}\dot{y} + \frac{1}{K}\left[\frac{8}{We} - \frac{8}{19} - \frac{2}{19}y\right]y = \frac{8}{19K} \tag{8}$$

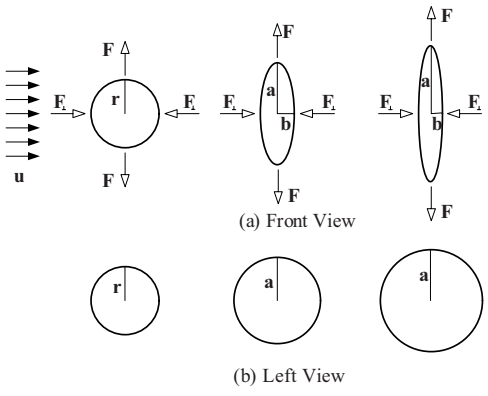

Fig. 3. Droplet deformation and external force in the APTAB model.

This equation is solved by the fourth order Runge-Kutta method.

The breakup criterion is given by

$$2(1+0.5y)^5+(1+0.5y)^{-1}-4(1+0.5y)^{-4}>C_bWe \tag{9}$$

3.2 Droplet size distribution function (Rosin-Rammler distribution)

The droplet size distribution was used to predict the droplet sizes of the children droplets after a parent droplet breakup in the hybrid breakup model. Therefore, in order to compute the vaporization and combustion process of the GDI spray accurately, the details of the droplet size distribution are very important. The x^2 distribution was used generally in previous breakup models. However, this distribution function results in overestimated population of large-size droplets. Therefore, in the present study, the Rosin-Rammler distribution was used instead of the x^2 distribution. The Rosin-Rammler distribution showed more accurate prediction ability for the droplet size in the high pressure swirl injector [14]. As shown in Fig. 4, the Rosin-Rammler distribution is relatively narrow compared with the x^2 distribution. This means that the x^2 distribution could overestimate the spray tip penetration due to large droplets.

The Rosin-Rammler cumulative distribution has the general form

$$V=1-\exp\left[-\left(\left(\frac{D}{\bar{D}}\right)^q\right)\right] \tag{10}$$

and the corresponding volume distribution is

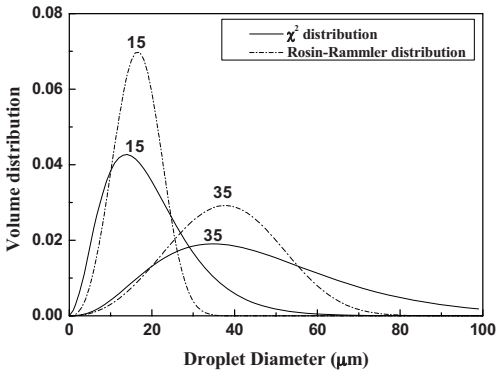

Fig. 4. Comparison of the x^2 distribution and the Rosin-Rammler distribution for two Sauter Mean Diameter (SMD) cases (Han et al. 1997).

$$\frac{dV}{dD}=\frac{qD^{q-1}}{\bar{D}^q}\exp\left[-\left(\frac{D}{\bar{D}}\right)^q\right] \tag{11}$$

where D is the size of the individual droplets. The distribution parameter, q, is set to 3.5 (Han, 1997).

$$\bar{D}=D_{32}\Gamma\left(1-q^{-1}\right) \tag{12}$$

where D_{32} is the droplet size diameter and is being used here to initialize the droplet size distribution. Γ is the gamma function, given by

$$\Gamma(x)=\int_0^\infty e^{-t}t^{x-1}dt \tag{13}$$

4. Results and discussions

The spray characteristics of a high-pressure swirl

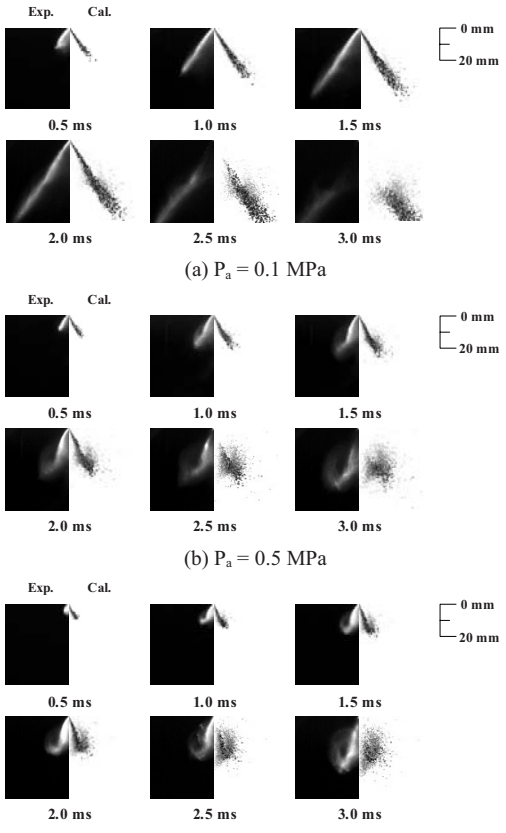

(a) P_a = 0.1 MPa

(b) P_a = 0.5 MPa

(c) P_a = 1.0 MPa

Fig. 5. Calculated and experimental spray development process at different ambient pressure (P_a = 0.1 MPa, 0.5 MPa, 1.0 MPa).

injector were analyzed by the numerical and experimental method at the ambient pressure of 0.1 MPa, 0.5 MPa and 1.0 MPa for the ambient temperature of 293 K.

Fig. 5 shows the calculated and experimental spray development process after the start of injection under the ambient pressure of 0.1 MPa, 0.5 MPa and 1.0 MPa. The left sides of the images show experimental results, and the right sides give the calculated ones. The calculated spray structures showed good agreement with the experimental results. In particular, the vortex cloud at the leading edge observed in the images by experiment was also captured in the calculation. The generation process of the vortex cloud at the spray tip can be explained by Fig. 6, in which the calculated gaseous flow field in the spray axis plane is shown with droplets. The spray motion causes the gas flow to circulate through the spray. The entraining gas flows interact with the spray droplets and suppress the spray development. The gaseous vortex flow also tends to carry the smaller spray droplets, hence, the generated vortex. The vortex was more clearly observed by increasing the ambient pressure. This phenomenon is due to a loss of momentum energy of the droplets due to high gas density under high ambient pressure conditions. These droplets follow the gaseous flow very well. The cone angle, the spray tip penetration and the spray width were also decreased by increasing the ambient gas pressure.

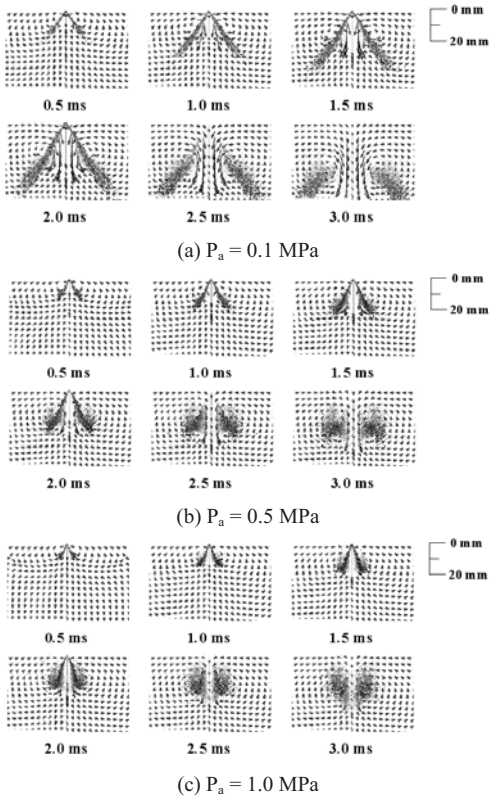

(a) P_a = 0.1 MPa

(b) P_a = 0.5 MPa

(c) P_a = 1.0 MPa

Fig. 6. Spray-induced gas entrainment according to time after injection (P_a = 0.1 MPa, 0.5 MPa, 1.0 MPa).

Fig. 7 shows calculated and experimental spray tip penetrations at the ambient pressure of 0.1 MPa, 0.5 MPa and 1.0 MPa. The experimental spray tip penetration was determined from the visible leading edge of the spray images, and the calculated one was defined as the average distance of the leading 20 particles from the injector nozzle. Congruent agreements between the calculation and experiment were obtained. At the early part after the start of injection, the spray tip penetration increased monotonously, and then it stagnated at a certain time due to the loss of droplet momentum. The spray tip penetration at high ambient pressure conditions was shorter than the one at low ambient pressure conditions due to a high density of ambient gas. The spray tip penetration at the ambient pressure of 0.5 MPa decreased about 33.1% by calculation and 33.7% by experiment compared with 0.1 MPa. At an ambient pressure of 1.0 MPa, it decreases to about 49.5% by calculation and 50.3% by experiment.

Fig. 8 shows the spray width at the ambient pressure of 0.1 MPa, 0.5 MPa and 1.0 MPa. The calculated results showed a similar tendency with the experimental ones. The spray width became shorter with the increase in ambient pressure. The differences of the spray width between 0.1 MPa and 0.5 MPa were about 41.2% by experiment and 42.7% by calculation. When the ambient pressure was increased to 1.0 MPa, the spray width decreased about 55.6%

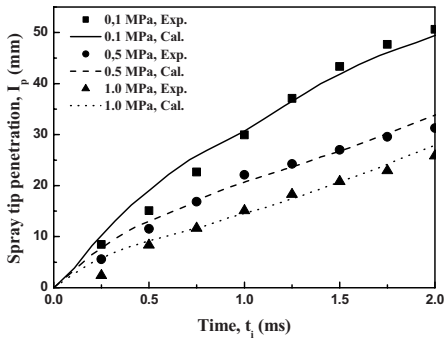

Fig. 7. Calculated and experimental spray tip penetration at different ambient pressure (P_a = 0.1 MPa, 0.5 MPa, 1.0 MPa).

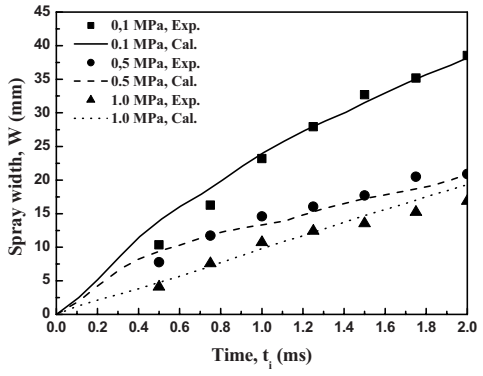

Fig. 8. Calculated and experimental spray width at different ambient pressure (P_a = 0.1 MPa, 0.5 MPa, 1.0 MPa).

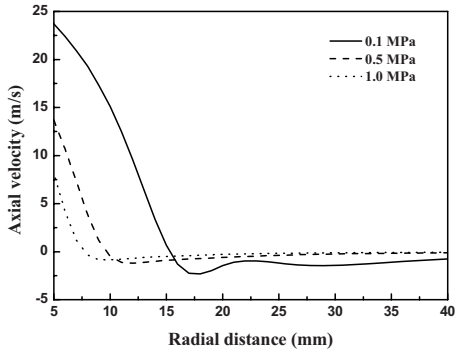

Fig. 9. Calculated axial gas velocity at 3.0 ms after injection and 30 mm downstream from the injector (P_a = 0.1 MPa, 0.5 MPa, 1.0 MPa).

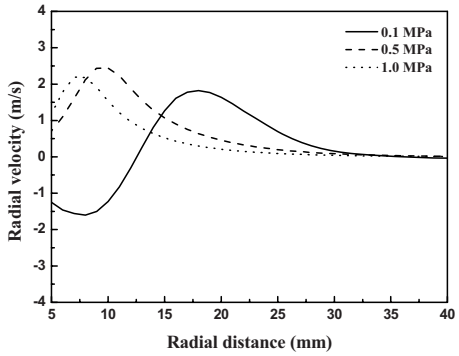

Fig. 10. Calculated radial gas velocity at 3.0 ms after injection and 30 mm downstream from the injector (P_a = 0.1 MPa, 0.5 MPa, 1.0 MPa).

by calculation and 56% by experiment. From Fig. 7 and Fig. 8, it was found that the spray tip penetrations and spray widths by calculation from 0 ms to 1.0 ms after the start of the injection were longer than the results of experiment. This is because the effects of the surrounding gas, liquid viscosity and surface tension before the breakup length in the LISA model for the primary breakup are ignored. Therefore, the droplets at the early time have larger size and momentum, which is why the calculated spray tip penetration is longer than experimental results.

Figs. 9 and 10 show calculated axial and radial gas velocity at the 30 mm downstream of the injector tip after 3.0 ms from the start of injection. In the case of the axial velocity, the positive value denotes the downstream direction. In the case of the radial velocity, the positive value denotes the outer direction. At an ambient pressure of 0.1 MPa, the axial gas velocity showed a maximum value at the center of the spray and it decreased as it went away from the spray center. A maximum negative velocity was observed at about 17 mm which results from the vortex ring. On the other hand, the radial velocity in the center of the spray showed a negative value and the velocity became positive from 13 mm of the radial distance. This means the vortex was generated near the 13 mm of the radial distance. The velocity profile at the ambient pressure of 0.5 MPa and 1.0 MPa were similar. The axial and radial velocities at the center of the spray were positive at the ambient pressure of 0.5 MPa and 1.0 MPa, which indicates that the vortex was generated at the inner area under high ambient pressures due to the high density of ambient gas. The axial velocity decreased with increasing the ambient pressure, and the position of upward vortex generation moved toward the center axis with increasing the ambient pressure. This indicates that the spray distributes near the center axis and the injector tip. Also, the maximum radial velocity moved toward the center axis by increasing the ambient pressure due to shorter spray widths at the high ambient pressures. The maximum value at the ambient pressure 0.1 MPa was smaller than the results at the ambient pressures of 0.5 MPa and 1.0 MPa. This phenomenon means that the spray at the ambient pressure 0.1 MPa is distributed more in the downstream region than that at the ambient pressures of 0.5 MPa and 1.0 MPa due to the longer spray tip penetration.

Fig. 11 shows SMD distribution in the 30 mm downstream from the injector tip obtained by calculation and experiment at 3.0 ms after the start of injection under various ambient pressure conditions. The calculated SMD distribution showed good agreements with the experimental results at an ambient pressure of 0.1 MPa. From the above results, we

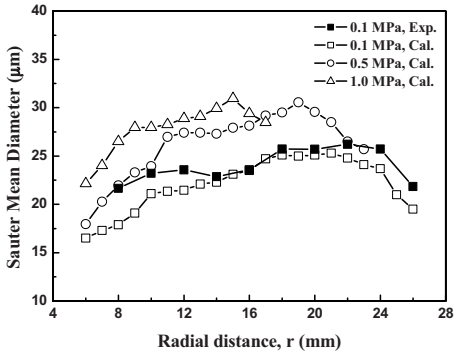

Fig. 11. Calculated and experimental SMD(Sauter Mean Diameter) at 3.0 ms after injection and 30 mm downstream from the injector (P_a = 0.1 MPa, 0.5 MPa, 1.0 MPa).

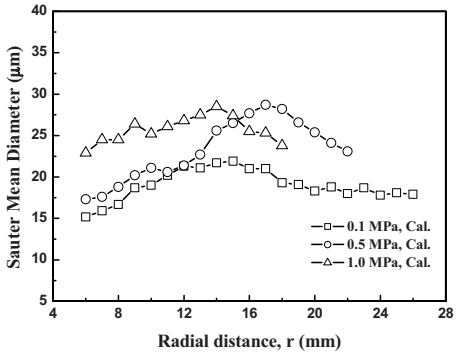

Fig. 12. Calculated and experimental SMD(Sauter Mean Diameter) at 4.0 ms after injection and 30 mm downstream from the injector (P_a = 0.1 MPa, 0.5 MPa, 1.0 MPa).

might expect reasonable calculated SMD even in high ambient pressure conditions such as 0.5 MPa and 1.0 MPa. SMD was smaller in the inner area of the spray and larger in the outer area. This is because the collision and coalescence of droplets prevent spray atomizing in the dense region of the spray.

Fig. 12 shows the computed SMD distribution in the 30 mm downstream from the injector tip at 4.0 ms after the start of injection. SMD was distributed wider than the one at 3.0 ms and the size became smaller due to atomization. The SMD was smaller at low ambient pressure conditions because atomization is more active due to wider spray dispersion at low ambient pressure conditions.

Table 2 represents the averaged SMD by calculation at 3.0 ms and 4.0 ms after injection. SMD was larger under high ambient pressure conditions, and it became smaller with the development of the spray. A difference of 14% at 0.1 MPa, 11% at 0.5 MPa and 8% at 1.0 MPa was observed.

Table 2. Calculated average SMD (Sauter Mean Diameter) (㎛).

Time \ Pressure	0.1 MPa	0.5 MPa	1.0 MPa
3.0 ms	22.1	26.2	27.8
4.0 ms	19.0	23.3	25.7

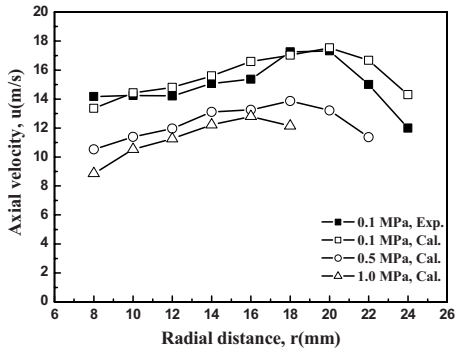

Fig. 13. Calculated and experimental axial velocity at 3.0 ms after injection and 30 mm downstream from the injector (P_a = 0.1 MPa, 0.5 MPa, 1.0 MPa).

Fig. 13 shows the calculated and experimental axial velocity of droplets at the various ambient pressures 30 mm downstream from the injector tip. However, the experiment was carried out only for the ambient pressure of 0.1 MPa due to the experiment limitation under the high ambient pressure conditions. The calculated results at the ambient pressure of 0.1 MPa showed good agreement with the experimental results. The axial velocity of the droplets was higher in the dense area of spray due to the higher momentum energy of the large droplets. At high ambient pressure conditions, the growth of the spray was weakened by ambient gas, and the droplet velocity became slower due to this phenomenon. The average droplet velocity at 0.5 MPa decreased to 30.2% of the result at 0.1 MPa, and a decrease of 50.1% was observed at 1.0 MPa.

5. Conclusions

The calculation and experiment of the spray characteristics of hollow-cone spray from high-pressure swirl injector were carried out at ambient pressures of 0.1 MPa, 0.5 MPa and 1.0 MPa for the ambient temperature of 293 K. The estimation of a new hybrid breakup model was performed. The LISA+APTAB model, which includes the Rosin-Rammler distribution function for the droplet size distribution, was used to calculate the spray structure.

used to calculate the spray structure. The Laser Induced Exciplex Fluorescence (LIEF) technique and Phase Doppler Anemometry (PDA) system were used for experimental measurements. The conclusions of this study are summarized as follows:

(1) A vortex cloud was seen at the spray tip, and the vortex more clearly appeared under high ambient pressure conditions. The spray growth was suppressed with increasing ambient pressure. The spray tip penetration and spray width became shorter at high ambient pressure.

(2) Calculated spray tip penetration and spray width showed a similar tendency with the experimental results by using the LISA+APTAB model.

(3) The axial droplet velocity was lower at the center of the spray and higher in the dense area of the spray with large SMD. At high ambient pressure conditions, the axial velocity was decreased.

(4) The effect on the SMD with spray development was discussed quantitatively. At high ambient pressure conditions, the SMD became larger.

(5) The LISA+APTAB model showed good prediction ability under the various ambient pressure conditions.

Nomenclature

a : Major semi-axis of an ellipsoidal cross section (㎛)
b : Minor semi-axis of an ellipsoidal cross section (㎛)
C_b : Dimensionless constant in the APTAB model, 0.5
d_0 : Injector exit diameter (㎛)
d_D : Droplet diameter (㎛)
d_L : Ligament diameter (㎛)
h : Sheet half thickness (㎛)
I_p : spray tip penetration (mm)
k_v : Velocity coefficient through injector
K : Density ratio of liquid and gas, ρ_l / ρ_g
K_L : The most unstable wave length on the ligaments
K_s : Wave number corresponding to the maximum growth rate
L : Breakup length (㎛)
$\dot{m}$: Mass flow rate (mg/s)
N : Dynamic viscosity ratio of liquid and gas, μ_l / μ_g
Δp : Pressure different across the injector (Pa)
r : Droplet radius at the equilibrium position (㎛)
Re : Reynolds number
t : Film thickness at the injector exit (㎛)
u : Axial component of sheet velocity (m/s)
U : Total sheet velocity (m/s)
W : Spray width (mm)
We : Weber number
y : Droplet distortion parameter

Greek symbols

μ : Dynamic viscosity (N/m·s)
θ : Spray angle (degree)
ρ : Density (kg/m^3)
σ : Gas-liquid surface tension coefficient
τ : Breakup time (s)
Ω : Growth of the most unstable wave

Subscripts

0 : At the injector exit
D : Droplet
g : Gas property
l : Liquid property
L : Ligament

Reference

[1] L. W. Evers, Characterization of transient spray from a high pressure swirl injector, *SAE paper* 940188 (1994).

[2] F. Zhao, J. Yoo, Y. Liu and M. Lai, Spray dynamics of high pressure fuel injector for DI gasoline engines, *SAE paper* 961925 (1996).

[3] C. Preussner, C. Doring, S. Fehler and S. Kampmann, GDI: interaction between mixture preparation, combustion system and injector performance, *SAE paper* 980498 (1998).

[4] R. B. Wicker, H. I. Loya, P. A. Hutchison and J. Sakakibara, SIDI fuel spray structure investigation using flow visualization and digital particle image velocimetry, *SAE paper* 1999-01-3535 (1999).

[5] D. S. Choi, D. J. Kim and S. C. Hwang, Development behavior of vaporizing sprays from a high-pressure swirl injector using exciplex fluorescence method, *KSME International Journal* 14 (10) (2000) 1143-1150.

[6] P. J. O'Rourke and A. A. Amsden, The TAB method for numerical calculation of spray droplet breakup, *SAE paper* 872089 (1987).

[7] E. A. Ibrahim, H. Q Yang and A. J. Przekwast,

Modeling of spray droplets deformation and break-up, *AIAA J. Propulsion and Power* 9 (4) (1993) 652-654.

[8] J. H. Park, Development of numerical spray models and application to aeropropulsion engines, Ph. D. Thesis, Seoul National University (2002).

[9] C. Beatrice, P. Belardini, C. Bertoli, M. C. Camerretti and N. C. Cirillo, Fuel jet models for multidimensional diesel combustion calculation : an update," *SAE paper* 950086 (1995).

[10] D. P. Schmidt, J. K. Martin and R. D. Reitz, Pressure-swirl atomization in the near field, *SAE paper* 1999-01-0496 (1999).

[11] S. W. Park, H. J. Kim, K. H. Lee and C. S. Lee, Atomization characteristics and prediction accuracy of LISA-DDB model for gasoline direct injection spray, *KSME International Journal* 18 (7) (2004) 1177-1186.

[12] C. A. Chryssakis, D. N. Assanis, J. K. Lee and K. Nishida, Fuel spray simulation of high-pressure swirl-injector for DISI engines and comparison with laser diagnostic measurements, *SAE Paper* 2003-01-0007 (2003).

[13] N. Dombrowski and W. R. Johns, The aerodynamic instability and disintegration of viscous liquid sheets, *Chem. Eng. Sci.* 18 (1963) 203-214.

[14] Z. Han, S. Parrish, P. V. Farrell and R. D. Reitz, Modeling atomization process of pressure-swirl hollow-cone fuel sprays, *Atomization and Sprays* 7 (1997) 663-684.